

Solitary waves on vortex lines in Ginzburg–Landau models

Natalia G. Berloff

*Department of Applied Mathematics and Theoretical Physics,
University of Cambridge, Wilberforce Road, Cambridge, CB3 0WA*

(Dated: June 25, 2004)

Axisymmetric disturbances that preserve their form as they move along the vortex lines in uniform Bose-Einstein condensates are obtained numerically by the solution of the Gross-Pitaevskii equation. A continuous family of such solitary waves is shown in the momentum (p) – substitution energy ($\hat{\mathcal{E}}$) plane with $p \rightarrow 0.09\rho\kappa^3/c^2$, $\hat{\mathcal{E}} \rightarrow 0.091\rho\kappa^3/c$ as $U \rightarrow c$, where ρ is the density, c is the speed of sound, κ is the quantum of circulation and U is the solitary wave velocity. It is shown that collapse of a bubble captured by a vortex line leads to the generation of such solitary waves in condensates. The various stages of collapse are elucidated. In particular, it is shown that during collapse the vortex core becomes significantly compressed and after collapse two solitary wave trains moving in opposite directions are formed on the vortex line.

An important role in the dynamics of nonlinear systems is played by solitary waves – the localised disturbances of the uniform field that are form-preserving and move with a constant velocity. They appear in diverse contexts of science and engineering, such as fluid dynamics, transport along macromolecules, fibre optic communications just to name few. Considerable interest attaches to determining the entire sequence of solitary waves as they define possible states that can be excited in the system. Understanding the production, motion and interactions of such solitary waves is one of the most significant questions in nonlinear science. In condensed matter systems solitary waves are topological objects since they owe their existence and perseverance to the topology of the order parameter field describing a medium with a broken symmetry. In this Letter I establish and study the production of a new class of solitary waves that move along vortex lines/topological defects in conservative Ginzburg–Landau systems. The discussion will be restricted to condensed matter system such as atomic Bose–Einstein condensates (BEC) where the evolution equation is the Gross – Pitaevskii (GP) model [1]; see equation (1) below (also known as defocusing nonlinear Schrödinger equation in nonlinear optics). The applications are not restricted to the condensed matter systems due to the generality of the Ginzburg–Landau systems with implications to the motion of excitations along cosmic strings in the early Universe [2] and along topological defects in other ordered media: liquid crystals [3], non-equilibrium patterns, etc. Finally, the new solutions to the nonlinear Schrödinger equation which this Letter presents are of interest when so few have been derived in multidimensions.

Symmetry-breaking transitions in equilibrium systems can be described by an energy functional, $\mathcal{E} = \int \mathcal{L} dV$, in terms of a Lagrangian \mathcal{L} . The simplest form of the Lagrangian, capable of describing the quenching beyond the critical point where the disordered state becomes unstable and the symmetry is spontaneously broken, is a Ginzburg-Landau Lagrangian $\mathcal{L} = \frac{1}{2}|\nabla\psi|^2 + \frac{1}{2}(1 -$

$|\psi|^2)^2]$ dependent on a complex scalar order parameter ψ . The evolution equation describing the relaxation to the equilibrium state in an energy-preserving (conservative) system is given by the Euler–Lagrange equation $\psi_t = -i\partial\mathcal{E}/\partial\psi^*$ that we write as

$$-2i\frac{\partial\psi}{\partial t} = \nabla^2\psi + (1 - |\psi|^2)\psi. \quad (1)$$

A phase singularity of a complex field ψ given by $\psi = 0$ is called a quantised vortex or topological defect depending on a particular application. The total change of phase around any closed contour must be a multiple of 2π and only quantised vortices with the total change of phase 2π are topologically stable.

Such a general reasoning gives a simple explanation why equation (1) has a universal meaning and has been applied to a variety of systems [4]. In particular, it described accurately both equilibrium and dynamical properties of BEC [5]. The GP model has been remarkably successful in predicting the condensate shape in an external potential, the dynamics of the expanding condensate cloud and the motion of quantised vortices; it is also a popular qualitative model of superfluid helium. For these systems equation (1) is written in dimensionless variables such that the unit of length corresponds to the healing length ξ , the speed of sound $c = 1/\sqrt{2}$, and the density at infinity $\rho_\infty = |\psi_\infty|^2 = 1$.

The straight-line vortex positioned along the z - axis is obtained by rewriting (1) in cylindrical coordinates (s, θ, z) and using the ansatz $\psi_0 = R(s)\exp(i\theta)$. The resulting solution for $R(s)$ was found numerically in the first reference of [1] and approximated in [6]. The infinitesimal perturbations of a rectilinear vortex in the GP model may be bound or free, depending on their angular and axial wavenumbers, m and k . The free waves radiate energy acoustically to infinity, while the bound states do not. The low frequency modes $m = 1$, that displace the axis of the vortex, are found to be bound for all k [7, 8]. The low frequency modes $m = 2$ are also bound when k is sufficiently large, but are free for small k [8].

A family of fully three-dimensional solitary waves was found by Jones and Roberts [9] who integrated (1) numerically and determined the entire sequence of solitary wave solutions of the GP equation, such as vortex rings and finite amplitude sound waves named rarefaction pulses. They showed the location of the sequence on the momentum, p , energy, \mathcal{E} , plane, that I shall refer to as the JR dispersion curve. In three dimensions they found two branches meeting at a cusp where p and \mathcal{E} assume their minimum values, p_m and \mathcal{E}_m . As $p \rightarrow \infty$ on each branch, $\mathcal{E} \rightarrow \infty$. On the lower branch the solutions are asymptotic to large vortex rings. As \mathcal{E} and p decrease from infinity along the lower branch, the solutions begin to lose their similarity to large vortex rings. Eventually, for a momentum p_0 slightly greater than p_m , they lose their vorticity (ψ loses its zero), and thereafter the solitary solutions may better be described as ‘rarefaction waves’. The upper branch consists entirely of these and, as $p \rightarrow \infty$ on this branch, the solutions approach asymptotically the rational soliton solution of the Kadomtsev-Petviashvili Type I equation.

In what follows I determine the entire family of axisymmetric ($m = 0$) solitary wave solutions that move along the straight-line vortex and relate them to the JR dispersion curve. In equation (1) written in cylindrical coordinates (s, θ, z) I take the ansatz $\psi = (R(s) + \phi(s, z)) \exp(i\theta)$, and assume that the disturbance $\phi(s, z)$ moves with velocity U in the positive z -direction. In the frame of reference moving with the solitary wave, $\phi(s, z)$ satisfies

$$2iU \frac{\partial \phi}{\partial z} = \frac{1}{s} \frac{\partial}{\partial s} \left[s \frac{\partial \phi}{\partial s} \right] + \frac{\partial^2 \phi}{\partial z^2} - \frac{\phi}{s^2} + (1 - 2R^2 - R(\phi + 2\phi^*) - |\phi|^2)\phi - R^2\phi^* \quad (2)$$

The disturbance is localised, so the boundary condition is $\phi(s, z) \rightarrow 0$, as $|\mathbf{x}| \rightarrow \infty$ in all directions of \mathbf{x} . In view of the asymptotic expansions at infinity [9], I introduce stretched variables $z' = z$ and $s' = s\sqrt{1 - 2U^2}$ and map the infinite domain onto the box $(0, \frac{\pi}{2}) \times (-\frac{\pi}{2}, \frac{\pi}{2})$ using the transformation $\hat{z} = \tan^{-1}(Lz')$ and $\hat{s} = \tan^{-1}(Ls')$, where L is a constant $\sim 0.1 - 0.4$. Transformed equation (2) was expressed in second-order finite difference form using 250x200 grid points, and the resulting nonlinear equations were solved by Newton-Raphson iteration procedure using banded matrix linear solver based on bi-conjugate gradient stabilised iterative method with preconditioning. For each solitary wave two quantities were calculated: the nonzero (z -) component of the momentum [9]

$$p = \frac{1}{2i} \int \left[\nabla \psi (\psi^* - 1) - \nabla \psi^* (\psi - 1) \right] dV \quad (3)$$

and the substitution energy, $\hat{\mathcal{E}}$, which is the difference between the energy of the vortex-solitary wave complex

and the energy of the vortex line,

$$\hat{\mathcal{E}} = \frac{1}{2} \int |\nabla \psi|^2 - |\nabla \psi_0|^2 + \frac{1}{2}(1 - |\psi|^2)^2 - \frac{1}{2}(1 - |\psi_0|^2)^2 dV. \quad (4)$$

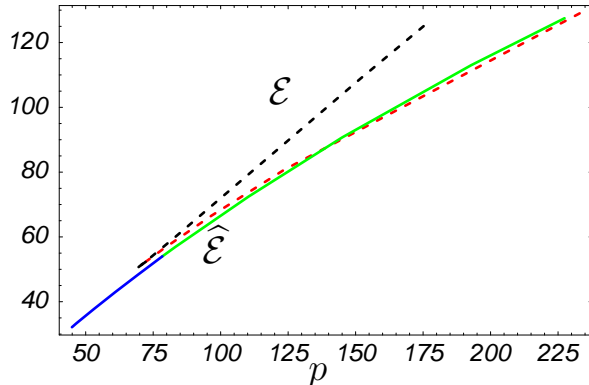
By performing the variation $\psi \rightarrow \psi + \delta\psi$ in (3)–(4) and discarding surface integrals that vanish provided $\delta\psi \rightarrow 0$ for $\mathbf{x} \rightarrow \infty$, we see that $U = \partial \hat{\mathcal{E}} / \partial p$, where the derivative is taken along the solitary wave sequence. The same expression is obeyed by the sequences of classical vortex rings in an incompressible fluid and by the solitary waves of [9]. I also note that if we multiply $\hat{\mathcal{E}}$ by $z \partial \psi^* / \partial z$ and integrate by parts we get $\hat{\mathcal{E}} = \int |\partial \psi / \partial z|^2 dV$, similarly to the expression for the energy of the JR solitons [10]. This expression was used as a check of the numerical accuracy. As $p \rightarrow \infty$, $\hat{\mathcal{E}} \rightarrow \infty$ and solitary wave solutions are represented by large vortex rings moving along the vortex line. As $\hat{\mathcal{E}}$ and p decrease from infinity, the radii of the rings decrease and for a momentum $p_0 \lesssim 78$, $\phi(s, z) = 0$ on z -axis only. To distinguish these solutions from vortex rings and to emphasise the analogy with the JR solitary waves, these solutions will be called rarefaction waves as well. Table 1 shows the velocity, substitution energy, momentum and radius of the solitary wave solutions found. Figure 1 shows the momentum-energy curve of the solutions in comparison with the JR dispersion curve. Notice that unlike the JR dispersion curve, there is no cusp on the energy-momentum plane. As $U \rightarrow c$ neither $\hat{\mathcal{E}}$ nor p go to infinity, instead $\hat{\mathcal{E}} \rightarrow 32$ and $p \rightarrow 45$ which lies below the JR cusp. The substitution energy, $\hat{\mathcal{E}}$, and momentum, p , of our vortex rings are larger than corresponding values of \mathcal{E} and p of the JR rings moving with the same velocity. If the vortex rings of the same radii are compared, our rings have lower energy and momentum. Figure 2 shows the density isoplots, the density contour plots, and the velocity vector fields of two representative solutions such as a rarefaction pulse and a vortex ring. Notice the vortex core expansion at the centre of the vortex ring due to a decrease in pressure in high velocity region.

Table 1. The velocity, U , substitution energy, $\hat{\mathcal{E}}$, momentum, p and radius, b , of the solitary wave solutions moving along the straight-line vortex.

U	0.4	0.45	0.5	0.55	0.6	0.61
$\hat{\mathcal{E}}$	142	113	90.7	72.4	56.9	54.0
p	262	193	145	110	83.2	78.4
b	4.18	3.62	3.08	2.41	1.05	0.1
U	0.63	0.65	0.67	0.69	0.7	0.75
$\hat{\mathcal{E}}$	48.4	43.0	37.8	33.3	32.2	32.1
p	69.4	61.0	53.1	46.5	45.0	45.0

A question that arises after new solutions are found theoretically is how to create them in an actual physical system. In [11] we established a new mechanism of vortex nucleation by collapsing bubbles in the context of the GP model. These results referred to collapse of cavitated

FIG. 1: (color online) The dispersion curves for two families of the axisymmetric solitary wave solutions. The dashed line represents the JR dispersion curve. The part of the curve that corresponds to the vortex rings is shown in grey (red). The solid line gives the substitution energy as a function of momentum for the solitary waves moving along the vortex line with vortex rings shown in light grey (green).

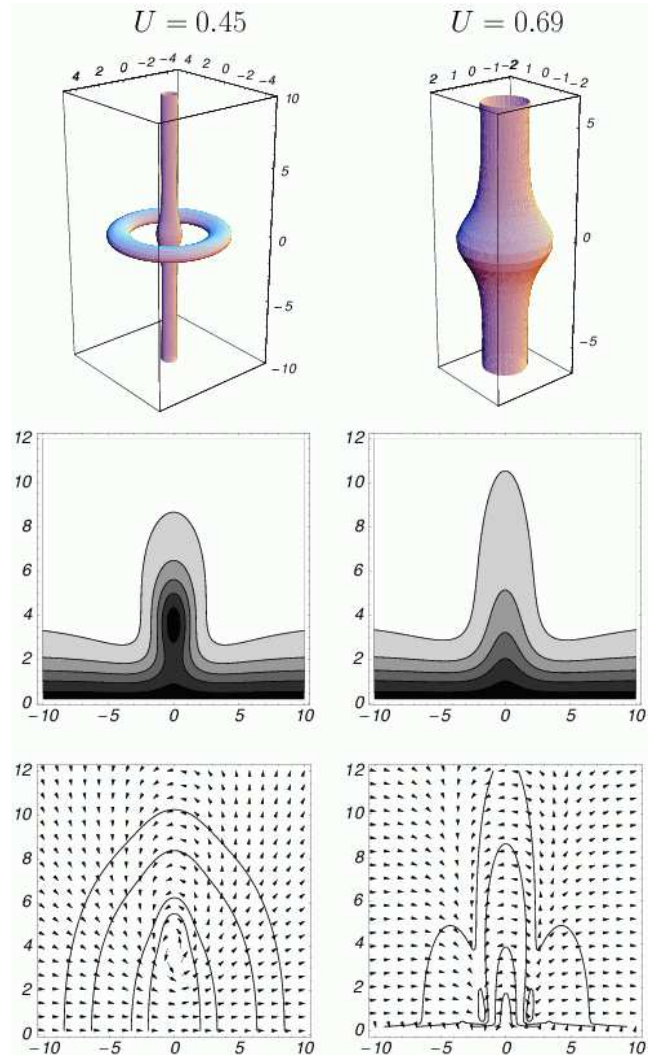


bubbles generated by ultrasound in the megahertz frequency range that have been observed to produce quantised vortices in superfluid helium [12]. Also, vortices form as a result of bubbles colliding during a first-order phase transition of an early Universe [2]. In [13] we have shown that a soft bubble, carved out in the surrounding fluid by an electron through its zero-point motion, becomes trapped in vortex lines. The Bernoulli effect of the flow created by the flow circulation around the vortex propels the bubble and vortex towards one another with a force approximately proportional to s^{-3} , where s is the closest distance between them. As the bubble becomes trapped in the vortex core, the flow round the bubble acquires circulation that it previously could not possess. After the emission of Kelvin waves, that were excited on the vortex core during the capture, the bubble-vortex complex stabilises to an axisymmetric form depicted in Figure 2 of [13]; see also Figure 3 ($t = 0$) below. One could expect that a similar capture of bubbles created by ultrasound takes place in BEC and that vacuum bubbles get trapped in cosmic strings. The captured bubble will then collapse sending axisymmetric waves along the vortex line. To elucidate the stages of this collapse I performed the numerical simulations of the GP equation (1) starting with the initial condition

$$\psi(\mathbf{x}, t = 0) = \begin{cases} R(s)e^{i\theta}\tanh\left(\frac{r-a}{\sqrt{2}}\right) & \text{if } r > a \\ 0 & \text{if } 0 \leq r \leq a, \end{cases} \quad (5)$$

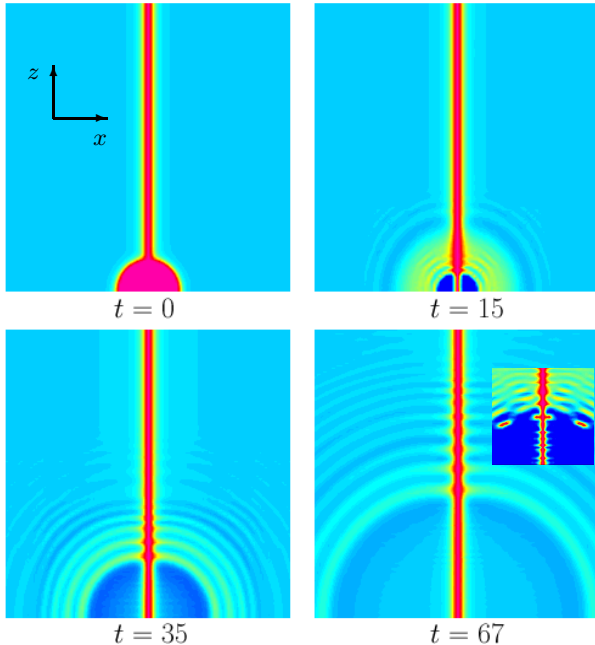
where $r^2 = x^2 + y^2 + z^2$. Initial state (5) gives an accurate representation of the stationary complex, that consists of the straight-line vortex at $x = 0, y = 0$ and the bubble of radius a centred at the origin. The surface of the bubble is assumed to be an infinite potential barrier to the condensate particles, so no bosons can be found inside

FIG. 2: (colour online) Two solitary wave solutions moving with velocity $U = 0.45$ (left side) and $U = 0.69$ (right side) along the straight-line vortex. The density isoplots at $\rho = 0.1$ (left) and $\rho = 0.3$ (right) are shown on two top panels. The density contour plots (0.1, 0.3, 0.5, 0.7, 0.9) at the cross-section $\theta = 0$ are shown on two middle panels. The velocity fields with contour plots (0.05, 0.1, 0.3, 0.5) of the velocity magnitude, $\sqrt{v_s^2 + v_z^2}$, are given at the bottom.



the bubble ($\psi = 0$) before the collapse, and this is why $\tanh(\ell/\sqrt{2})$, which is the wavefunction of the condensate distance ℓ away from a solid wall, is relevant here. ‘Softer’ bubbles that allow some condensate penetration were also considered by reducing the slope of the hyperbolic tangent, but no significant difference was detected. I performed fully three-dimensional calculations for cavities of various radii in a computational cube with sides of 200 healing lengths [14]. Figure 3 shows the density plots of the portion of the cross-section at $y = 0$ at various times after the collapse of a bubble of radius $a = 10$. Figure 4 depicts density contours $\rho/\rho_\infty = 4/5$ at times $t = 0, 20$ and 60. The time-dependent evolution of the

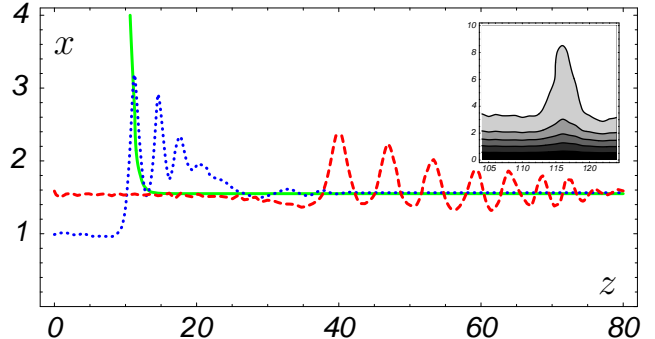
FIG. 3: (colour online) Collapse of the bubble of radius $a = 10$ trapped by the vortex line. The density plots of the cross-section of the solution of (1) with initial state (5) at $y = 0$, $x \in [-50, 50]$, $z \in [0, 100]$ are shown. The insert shows a vortex ring travelling along the z -axis generated after collapse of the bubble of radius $a = 50$ at $t = 100$. Two vortex rings of smaller radii are also seen on the left and on the right of it. Both low and high density regions are shown in darker shades to emphasise intermediate density regions.



condensate during and after bubble's collapse involves several stages. During the first stage dispersive and non-linear wave-trains are generated at the surface of the bubble. This stage of the evolution is characterised by a flux of particles towards the centre of the cavity. This creates an inward force acting on the vortex core reducing the cross-sectional area of the core. The reduction by a factor of 1.5 is seen on $t = 15$ snapshot of Figure 3 and on the density contour of Figure 4 at $t = 20$. The next stage in the evolution is outward expansion of the condensate that overfilled the cavity. The instability mechanism for collapsing bubbles in the absence of the straight-line vortex, which we described in detail in [11], sets in, leading to the production of vortex rings and rarefaction pulses mostly along the vortex line, as the energy and momentum necessary for their creation is lower there. As the train of solitary waves starts moving away from the collapsed bubble (see Figures 3 and 4), the distance between them increases since they move with different velocities. In time each individual solitary wave approaches its localised form found in the first part of this paper; see the insert of Figure 4. During collapse of a bubble of a larger radius ($a \gtrsim 28$) vortex rings will be generated together with rarefaction pulses on the vortex line; see the insert of Figure 3.

The author is grateful to Professors Paul Roberts

FIG. 4: (colour online) Collapse of the bubble of radius $a = 10$. The contour $\rho/\rho_\infty = 4/5$ is shown at $t = 0$ (green solid line), $t = 20$ (blue dotted line), and $t = 60$ (red dashed line). The density contour plot of the condensate showing a well-separated solitary wave at $t = 166$ is given in the insert (compare this with the middle right panel of Figure 2).



and Boris Svistunov for useful comments about this manuscript. The support from NSF grant DMS-0104288 is acknowledged.

-
- [1] V.L. Ginzburg and L.P. Pitaevskii, Zh. Eksp.Theor. Fiz. **34** 1240 (1958) [Sov. Phys. JETP **7** 858 (1958)]; E.P. Gross, Nuovo Cimento **20** 454 (1961)
 - [2] A. M. Srivastava, Phys. Rev. D **46** 1353 (1992); G.E Volovick, Phys. Rep.-Rev. Sec. Phys. Lett. **351** 195 (2001); K. Kasamatsu and M. Tsubota, J. Low Temp. Phys. **126** 315 (2002)
 - [3] I. Chuang, N. Turok, and B. Yurke, Phys. Rev. Lett. **66** 2472 (1991)
 - [4] L.M. Pismen "Vortices in nonlinear fields: from liquid crystals to superfluids: from non-equilibrium patterns to cosmic strings," Clarendon Press, Oxford (1999)
 - [5] A. L. Fetter and A. A. Svidzinsky J. Phys.: Condens. Matter **13** R135 (2001)
 - [6] N. G. Berloff, J. Phys. A: Math. Gen. **37** 1617 (2004)
 - [7] L.P. Pitaevskii, Sov. Phys. JETP **13** 451 (1961)
 - [8] P. H. Roberts, Proc. R. Soc. Lond. **459** 597 (2003)
 - [9] C. A. Jones and P. H. Roberts, J. Phys. A: Gen. Phys. **15** 2599 (1982).
 - [10] C. A. Jones, S. J. Putterman, and P. H. Roberts, J. Phys. A: Math. Gen. **19** 2991 (1986)
 - [11] N.G. Berloff and C.F. Barenghi, submitted to Phys. Rev. Lett, cond-mat/0401021.
 - [12] R.D. Finch, R. Kagiwada, M. Barmatz and I. Rudnick, Phys. Rev. A **134** 1425 (1964); R.F. Carey, J.A. Rooney and C.W. Smith, Phys. Lett. A **65** 311 (1978)
 - [13] N.G. Berloff and P. H. Roberts, Phys. Rev. B **63** 024510 (2000)
 - [14] I used the same numerical method as in work [15]. The faces of the computational box were open to allow sound waves to escape.
 - [15] N. G. Berloff and P. H. Roberts, J. Phys.: Math. Gen. **33** 4025 (2000)